Mon. Not. R. Astron. Soc. **000**, 1–9 (2003) Printed 2 February 2008 (MN LATEX style file v2.2)

Evidence for a multi–zone warm absorber in the XMM–Newton spectrum of Markarian 304

E. Piconcelli[1⋆], E. Jimenez-Bailón[1], M. Guainazzi[1], N. Schartel[1], P.M. Rodríguez-Pascual[1], M. Santos-Lleó[1]
[1] *XMM-Newton Science Operation Center/RSSD–ESA, Apartado 50727, Madrid 28080, Spain*

Accepted. Received

ABSTRACT

We present a *XMM–Newton* observation of Markarian 304, a Seyfert 1 galaxy at $z = 0.066$. The *EPIC* data show that MKN 304 is affected by heavy ($N_H \approx 10^{23}$ cm^{-2}) obscuration due to ionized gas. A two–phase warm absorber provides an adequate parameterization of this gas. The ionization parameter of the two components is $\xi \approx 6$ erg cm^{-2} s^{-1} and $\xi \approx 90$ erg cm^{-2} s^{-1}, respectively. The observed continuum photon index ($\Gamma \approx 1.9$) is typical for Seyfert 1 galaxies. Two significant emission lines are detected at 0.57 keV and 6.4 keV, respectively. The former is mostly likely due to He–like oxygen triplet emission arising from an ionized plasma (maybe the warm absorber itself). The latter is due to fluorescent emission of K–shell iron in a low–ionization state (FeI–XV). The upper limit for the line width of $\sigma_{K\alpha} < 0.18$ keV most likely rules out an origin in the inner parts of the accretion disk. Interestingly, the strength of such line is consistent with the possibility that the emission is produced in the warm absorber itself. However, a substantial contribution from the torus is plausible too. We have also found a weak (4% of the primary continuum) soft excess emission component. The presence of this excess could be explained by either emission/scattering from a warm gas or partial covering, or a combination of them.

Key words: galaxies: active – galaxies: individual: Markarian 304 – galaxies: Seyfert – X–rays: galaxies.

1 INTRODUCTION

The bulk of the X–ray emission in active galactic nuclei (AGNs) is produced via Comptonization of UV photons in the inner parts of the accretion flow close to the central supermassive black hole. The resulting power law spectrum is modified by a number absorption and emission spectral features due to the reprocessing of this primary continuum (Mushotzky, Done & Pounds 1993). They are clear signatures of the presence of large amounts of gas characterized by different physical properties in the circumnuclear region.

One of the most common spectral features is the so–called *warm* (i.e. partially ionized) *absorber* (Halpern 1984; Pan et al. 1990, Turner et al. 1993). Such a component has been found to contribute significantly to the opacity of the X–ray primary emission in $\approx 50\%$ of the Seyfert 1 galaxies with column densities up to $\gtrsim 10^{23}$ cm^{-2} (Reynolds 1997). In particular, OVII (0.739 keV) and OVIII (0.871 keV) absorption edges resulted to be the most prominent absorption signatures of the ionized gas in low–resolution *ASCA* observations.

The advent of grating spectrometers on–board *XMM–Newton* and *Chandra* has dramatically enriched our knowledge in this field. High–resolution soft X–ray spectra of bright Type 1 AGNs present a wealth of absorption lines (e.g. Collinge et al. 2001; Kaspi et al. 2001; Kaastra et al. 2002), which allow to infer a few remarkable conclusions: (*i*) warm absorbers usually show a very complex structure, with multiple regions characterized by different ionization states, column densities and velocities; (*ii*) the strongest features are due to He– and H–like states of O, Ne, Mg and Si; in addition a blend of M–shell iron inner shell transition (unresolved transition array or UTA) has been often detected in the range ≈ 0.70–0.80 keV; (*iii*) the observed blueshift of the absorption lines imply they are originated in an outflow with mean velocities in the range ≈ 100–2500 km/s.

However, two important issues regarding the warm absorbers still remain open, i.e.: the exact location of the absorbing medium and the physical connection between the absorbing materials in the UV and X–ray band. A likely

⋆ E-mail: epiconce@xmm.vilspa.esa.es

range of distances of the ionized absorbing medium from the central source is $r \approx 0.01$–10 pc (Krolik 2002; Behar et al. 2003).

By correlating *HST* and *ASCA* data Crenshaw et al. (1999) found that all Seyfert galaxies with evidence of UV absorption also exhibit X–ray ionized absorption features. Furthermore, some sources in which UV and X–ray absorbing components share the same outflow velocity space have been observed (Blustin et al. 2003; Collinge et al. 2001; Kaastra et al. 2002). However, no clearcut identification of an X–ray warm absorber with an UV counterpart has been reported yet (see Crenshaw, Kraemer & George 2003 for a review).

Unfortunately, the sensitivity of current grating spectrometers allows us to analyze just a handful of very bright X–ray sources. Therefore CCD cameras spectroscopy still represents the best available tool to deduce information about the physical properties of the gas in the immediate surroundings of the central X–ray emitting region for most AGNs (i.e. those with a $F_{2-10} \lesssim 1$ mCrab[1]). We present here the analysis of an *EPIC* observation of Markarian 304 ($F_{2-10} \approx 0.1$ mCrab).

Markarian 304 (MKN 304, PG2214+139) is a Seyfert galaxy at $z = 0.066$. Due to the presence of broad emission lines in its optical spectrum, MKN 304 has been classified as a Type 1 object (Osterbrock 1977). *IUE* spectroscopy of this source revealed the presence of strong bump in the UV (Clavel & Joly 1984), without absorption lines. On the contrary, a recent *FUSE* observation of MKN 304 (Kriss 2002) disclosed broad absorbing features (with a velocity spread of 1500 km/s) due to multiple OVI absorption components blended together.

MKN 304 was discovered as X–ray emitting source by *Uhuru* (Tananbaum et al. 1978). Later X–ray observations of this source were performed by *Einstein* (Kriss, Canizares & Ricker 1980) and *ROSAT* (Rachen et al. 1996): both reported evidences of heavy obscuration, with a very flat slope ($\Gamma \sim 0.07$) in the soft X–ray band. Surprisingly, MKN 304 was not targeted by *ASCA* and *BeppoSAX* and, therefore, no further study of its unusual flat continuum was performed.

Throughout this paper we assume a flat ΛCDM cosmology with ($\Omega_{\rm M}$,Ω_{Λ}) = (0.3,0.7) and a Hubble constant of 70 km s^{-1} Mpc^{-1} (Bennett et al. 2003).

2 *XMM–Newton* OBSERVATIONS AND DATA REDUCTION

MKN 304 was observed by the European Photon Imaging Camera (*EPIC*) on board the *XMM–Newton* space observatory (Jansen et al. 2001) between 2002 May 12 15:46:29 (UT) and 2002 May 13 00:56:34 (UT). The observation was performed with the *EPIC PN* camera (Struder et al. 2001) operating in Full Window Extended mode and with the *EPIC MOS* cameras (Turner et al. 2001) operating in Full Window mode. All the three *EPIC* cameras were equipped with the "Thin" blocking optical filters.

[1] 1 Crab corresponds to a 2–10 keV flux of $\sim 2 \times 10^{-8}$ erg cm^{-2} s^{-1}.

The data files were reduced and analyzed using the standard Science Analysis System (*SAS*) v.5.4.1. We used the EPCHAIN and EMCHAIN tasks for processing of the raw *PN* and *MOS* data files, respectively, in order to generate the relative linearized event files. X–ray events corresponding to patterns 0–12 (i.e. single–, double–, triple–, and quadruple–pixel events) for the *MOS* cameras were selected; for the *PN*, patterns 0–4 events (i.e. single– and double–pixel events) were used. The subsequent event selection was carried out taking into account the most updated calibration files at the time the reduction was performed (September 2003). All known flickering and bad pixels were removed. The event lists were furthermore filtered to ignore periods of high background flaring (see Appendix A). After this screening process (and taking into account satellite dead times) the effective net exposure times for the *MOS1*, *MOS2* and *PN* detectors are 33.4, 35.5 and 29 ks, respectively. No exposure is affected by pile–up. The peak of the X–ray emission is located at $\alpha_{2000} = 22^h17^m12.1^s$ and $\delta_{2000} = +14^\circ14'21.7''$, i.e. at a distance of 1.5 arcsecs from the coordinates of the optical nucleus of MKN 304 (Clements 1981). This is consistent with typical attitude reconstruction uncertainties.

Since the cleaned *RGS* data did not yield enough photons for a meaningful spectral analysis, they are not discussed in the following.

The source spectra were extracted from the final filtered event lists using a circular region of 24 and 21.5 arcsecs radius for *PN* and *MOS*, respectively, centered on the observed position of MKN 304. Backgrounds were estimated from source–free similar regions close to the source on the same CCD. Response matrices and ancillary response files were generated using the RMFGEN and ARFGEN tools in the *SAS* software. Since difference between the *MOS1* and *MOS2* response matrices are a few percent, we created a combined *MOS* spectrum and response matrix. The *PN* and *MOS* spectra were then fitted simultaneously. Both spectra were grouped to give a minimum of 40 counts per bin in order to apply χ^2 statistics. Given the current calibration uncertainties and the detector sensitivities, events outside the 0.3–12 keV range were ignored in the *PN* spectrum, while, for the *MOS*, we retained the 0.6–10 keV band.

3 X–RAY SPECTRAL ANALYSIS

Spectral analysis was performed using XSPEC v.11.2 (Arnaud 1996). All the models presented in this Section and in the following one include absorption due to the line–of–sight Galactic column of $N_{\rm H} = 4.96 \times 10^{20}$ cm^{-2} (Dickey & Lockman 1990). The photoelectric absorption cross sections were taken from Morrison & McCammon (1983). The quoted errors refer to the 90% confidence level for one interesting parameter (i.e. $\Delta\chi^2 = 2.71$; Avni 1976).

The 0.5–2 keV and 2–10 keV *PN* lightcurves were visually inspected for checking variability. We did not detect any significant change in both count rates during the ≈ 9 hr observation.

We first fitted the *EPIC* spectra with a power law model in the 2–12 keV band. This simple model yielded a very poor fit ($\chi^2(\nu)$= 469(256)) and an extremely flat photon index of $\Gamma \approx 0.95$. Indeed the convex shape of the data–to–model

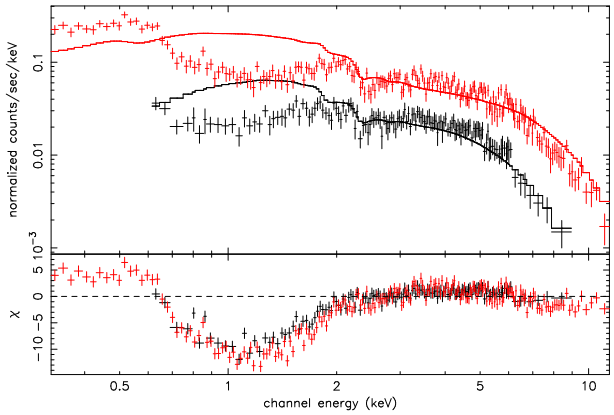

Figure 1. *Upper panel*: Continuum power law fit to the 2–12 keV band of the *PN* (top) and *MOS* (bottom) spectra of MKN 304, extrapolated over 0.3–12 (0.6–12) keV for *PN*(*MOS*). *Bottom panel*: Residuals in units of standard deviations.

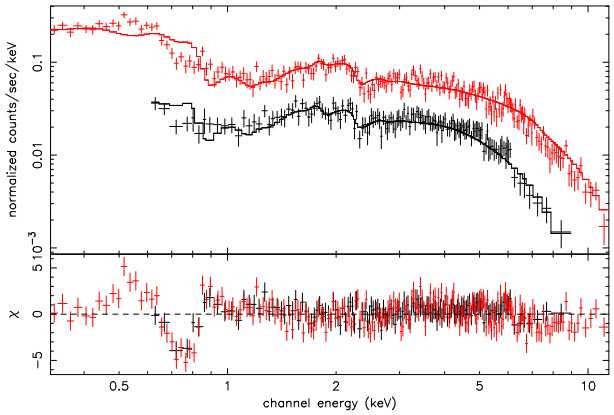

Figure 2. *Upper panel*: The *PN* (top) and *MOS* (bottom) spectra of MKN 304 fitted by a single warm absorber model (model B in Table 1). *Bottom panel*: Residuals in units of standard deviations. They clearly indicate that this model cannot account for the complex spectrum of MKN 304.

residuals suggests the presence of heavy obscuration. Fig. 1 displays the results of this fit extrapolated over the 0.3–12 keV bandpass. The large deficit in the 0.5–2 keV band clearly indicates the presence of a strong absorption, while the systematic positive residuals at $\lesssim$ 0.6 keV may reveal an emission component in excess of the underlying absorbed continuum. Fitting the data over the 0.3–12 keV band with a power law yielded a $\chi^2(\nu) = 2483(367)$ (see model A in Table 1).

We thus accounted for this ionized absorber component with the multiplicative **absori** model in XSPEC (Done et al. 1992). In this model the state of the warm absorber is a function of the ionization parameter ξ defined as $\xi = L/nr^2$, where L is the isotropic luminosity of the ionizing source in the interval 5 eV to 300 keV, n is the number density of the warm plasma and r is the distance between this latter and the central source. In the fit solar elemental abundances were assumed and ξ was left as a free parameter. On the contrary, we fixed the temperature of the absorber to T = 1.5 $\times$ 10^5 K since the statistics did not allow to simultaneously and effectively constrain T and ξ. Such a value of T falls in the typical range observed for a warm absorber (Reynolds & Fabian 1995; Krolik 2002 and reference therein). We also performed a further set of fits assuming values of temperature in the range $5 \times 10^4 < T < 10^6$ K, from which turned out that the ionization parameter remains almost constant (i.e. $\xi \approx$ 90–100 erg cm^{-2} s^{-1}) to the variations of temperature. This fit (indicated as model B in Table 1) resulted in a dramatic statistical improvement i.e. at $>$ 99.99% confidence level according to an F–test once compared to model A, with a $\chi^2(\nu) = 617(365)$. Nevertheless, the value of $\chi^2/\nu \approx 1.7$ remains unacceptable and a large absorption feature is evident in the soft portion of the spectrum (see Fig. 2). The breadth and depth of this feature suggest the existence of another ionized absorption component with a different value of ξ. Furthermore the derived slope $\Gamma = 1.40 \pm 0.04$ is significantly flatter than usually observed in unabsorbed Seyfert galaxies (Malizia et al. 2003) and quasars (Piconcelli et al. 2003), i.e. $\langle\Gamma\rangle \approx 1.9$.

We then added another **absori** component in the spectral model. First we fitted the spectrum fixing the temperature of this new component to the same value of the previous one, i.e. T = 1.5 $\times$ 10^5 K. The fit gave a minimum $\chi^2(\nu) =$ 477(363), with a statistical improvement significant at $>$ 99.99 confidence level. However, an even better χ^2 value (χ^2 = 441) was obtained fixing the temperature of the second ionized component to a lower value, in particular with T = 3 $\times$ 10^4 K. The resulting spectral parameters of this fit (Model C) are also listed in Table 1. The χ^2 value was reduced by $\Delta\chi^2 = 176$ respect to Model B, thus the addition of the low-temperature ionized absorption term is significant at a level larger then 99.99% confidence level (F–test value = 72).

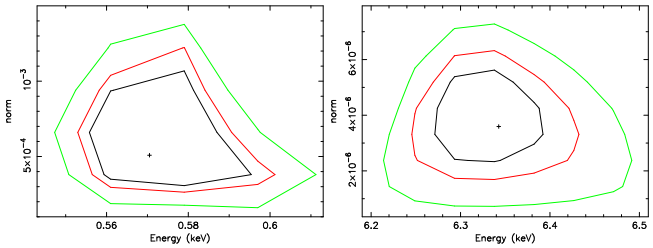

Figure 3. *Left panel*: contours at the 68%, 90% and 99% confidence level for energy and flux of the He–like oxygen line. *Right panel*: contours at the 68%, 90% and 99% confidence level for energy and flux of the iron line. Both fluxes are in units of photons/cm^2/s.

However the reported value of χ^2/ν = 1.22 (null hypothesis probability 0.003) is not yet very satisfactory and positive systematic residuals are still present in the data–to–model ratio below 1 keV.

We added a second power law accounting for this additional soft X–ray emitting component. The relative photon index was constrained to be that of the primary continuum but the normalization was left free to vary.

We obtained again a very significant improvement in the fit quality at the $>$ 99.99% confidence level (F–test = 66) with reduced χ^2 = 373 for 362 degrees of freedom (see

Model	Γ	N_H^{T5} (10^{22} cm^{-2})	ξ^{T5} (erg cm^{-2} s^{-1})	N_H^{T4} (10^{22} cm^{-2})	ξ^{T4} (erg cm^{-2} s^{-1})	Line Energy (keV)	χ^2(d.o.f.)
A	$0.58^{+0.02}_{-0.02}$	–	–	–	–	–	2483(367)
B	$1.40^{+0.04}_{-0.04}$	$6.4^{+0.3}_{-0.3}$	$92.9^{+9.8}_{-9.7}$	–	–	–	617(365)
C	$1.64^{+0.06}_{-0.06}$	$8.2^{+0.7}_{-0.7}$	$110.8^{+8.4}_{-7.7}$	$0.55^{+0.08}_{-0.08}$	$3.8^{+2.6}_{-1.4}$	–	441(363)
D	$1.92^{+0.08}_{-0.08}$	$10.9^{+0.9}_{-1.0}$	$112.7^{+29.0}_{-17.5}$	$1.3^{+0.3}_{-0.3}$	$2.9^{+1.2}_{-0.9}$	–	372(362)
E	$1.88^{+0.04}_{-0.04}$	$8.9^{+0.5}_{-0.5}$	$89.3^{+13.9}_{-12.0}$	$1.7^{+0.2}_{-0.4}$	$5.9^{+2.4}_{-0.9}$	$6.34^{+0.06}_{-0.06}/0.57^{+0.02}_{-0.01}$	335(358)

Table 1. X–ray spectral model fitting results. Parameters marked with T5(T4) are referred to the high–(low–) temperature component of the warm absorber. In model E the photon index of the unabsorbed power law was fixed to the value of the primary absorbed continuum. See text for details.

model D in Table 1). The resulting photon index is $\Gamma = 1.92\pm0.08$ and the normalization of the unabsorbed power law is $\approx 4\%$ of the absorbed power law component. The best fit column densities of the two ionized absorbers increased to $N_H^{T4} = 1.3\pm0.3 \times 10^{22}$ cm^{-2} and $N_H^{T5} = 10.9^{+0.9}_{-1.0} \times 10^{22}$ cm^{-2} for the lukewarm (i.e. with T = 3×10^4 K) and hot (i.e. with T = 1.5×10^5 K) component, respectively. The ionization parameters turn out to be $\xi^{T4} = 3.8^{+2.6}_{-1.4}$ erg cm^{-2} s^{-1} and $\xi^{T5} = 110.8^{+8.4}_{-7.7}$ erg cm^{-2} s^{-1}.

We attempted an alternative fit modelling the soft excess with a blackbody component attenuated by both ionized absorbers, and with all fit parameters free to vary, which yielded a minimum $\chi^2(\nu) = 399(361)$ and, therefore, significantly worse than model D. We also tried to substitute the "lukewarm" ionized absorbing component in model D with a neutral one, but the quality of the fit resulted very poor with a final $\chi^2(\nu) = 532(363)$ (null hypothesis probability 1.5×10^{-8}).

Model D provides an excellent and physically plausible parametrization of the overall *EPIC* spectrum of MKN 304, with a null hypothesis probability equal to ≈ 0.5. Visual inspection of the data–to–model ratio residuals suggests the presence of two emission features, respectively, at ~ 6 keV and ~ 0.5 keV (observer–frame). The former is likely due to the fluorescence emission from the iron K–shell as commonly observed in most of Seyfert galaxies (Nandra et al. 1997). The latter is likely due to the helium–like oxygen triplet of emission lines centered at 0.57 keV (rest–frame) as found in other Seyfert galaxies (e.g. Kaastra et al. 2002). Thus the data led us to add two narrow gaussian lines in model D to account for them. The best fit rest-frame energy of the Fe Kα line is 6.34±0.06 keV with an equivalent width of EW = 79±35 eV. This line is significant at 99.9% confidence level ($\Delta\chi^2 = 13$ for two additional parameters; F–test value = 7.3), the centroid energy corresponds to low ionization states, i.e. FeI–XV (Makishima 1986). We obtained an upper limit for the line width of $\sigma_{K\alpha} < 0.18$ keV. The rest–frame position of the soft X–ray line ($E = 0.57^{+0.02}_{-0.01}$ keV) is fully consistent with OVII emission. Given the reduction of χ^2 of $\Delta\chi^2 = 25$ for two additional degrees of freedom, the detection of this line is significant at $> 99.99\%$ confidence level based on an F–test. In Fig. 3 are shown the 68.3%, 90% and 99% confidence levels for two interesting parameters between the line energy and the flux of both emission features assuming model E in Table 1.

Fig. 4 shows the *PN* and *MOS* spectra and the spectral fit which includes the two gaussian emission line. We consider this spectral model (Model E in Table 1)as the best fit

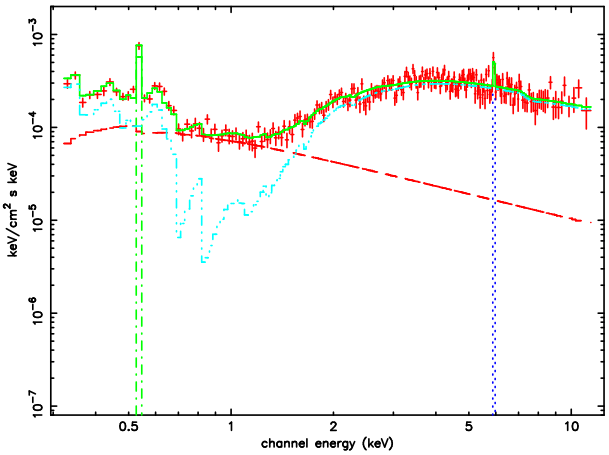

Figure 4. Unfolded best–fitting *EPIC* spectrum of MKN 304 fitted with two power laws plus a double warm absorber component and two gaussian lines (model E in Table 1). The photon index of the unabsorbed power law is fixed to the value of the primary absorbed continuum (see text for details).

to the *EPIC* data of MKN 304. This fit yields a minimum $\chi^2(\nu) = 335(358)$ with a null hypothesis probability of 0.82.

Once Model E was assumed, we measured a flux of $F_{0.5-2} = 3.06 \times 10^{-13}$ erg cm^{-2} s^{-1} and $F_{2-10} = 3.26 \times 10^{-12}$ erg cm^{-2} s^{-1} in the low (0.5–2 keV) and high (2–10 keV) energy bands, respectively. After correction for both Galactic absorption and warm absorber column densities, these correspond to luminosities of $L_{0.5-2} = 3.9 \times 10^{43}$ erg s^{-1} and $L_{2-10} = 4.8 \times 10^{43}$ erg s^{-1}, respectively. During the *XMM–Newton* observation the soft X-ray flux of MKN 304 was therefore a factor of 0.5 lower than measured[2] by *Einstein* on 1979 and a factor of 1.4 higher than the value obtained by *ROSAT* on 1992. Unfortunately, due to the lack of spectral information we cannot investigate the possibility that these variations are linked to changes in the column density of the observer or, alternatively, caused by the activity cycle of the X–ray continuum source.

[2] In order to compare the fluxes measured by different satellites we assumed a power law model with $\Gamma = 1.8$ and $N_H = N_H^{Gal}$.

4 DISCUSSION

The spectrum of MKN 304 unveiled by the *XMM–Newton* observation discussed in this paper is complex both in the soft and in the hard energy band (Fig. 1).

Our analysis fully confirms previous results on narrower energy ranges which reported a very flat continuum for this source, and suggested the existence of heavy obscuration. However, due to the limited bandpass and the poor sensitivity of the previous observations, it was impossible to accurately investigate the properties of the absorption, and discriminate between a cold (neutral) or warm (ionized) medium. This *XMM–Newton* observation of MKN 304 has clearly revealed that the strong obscuration ($N_H \approx 10^{23}$ cm^{-2}) occurs in an ionized gas.

We have indeed found that the best fit model to the *EPIC* data consists of a two–phase warm absorber with a high– and a low–ionized component, a faint soft excess component and two emission lines at ~ 0.57 keV and ~ 6.4 keV, respectively (see Model E in Table 1).

4.1 Warm absorber

We fixed *a priori* the temperature values at T = 1.5×10^5 K and T = 3.0×10^4 K for the two "phases" of the ionized plasma since they represent typical values observed in sources with a multi–phase warm absorber (Netzer et al. 2003; Kaastra et al. 2002). From the spectral analysis we derived $\xi^{T5} = 89.3^{+13.9}_{-12.0}$ erg cm^{-2} s^{-1} and $\xi^{T4} = 5.9^{+2.4}_{-0.9}$ erg cm^{-2} s^{-1} for the hot and the cold component, respectively (see model E in Table 1).

Our findings for MKN 304 appear to be in agreement with a "multi–zone" structure for the ionized absorber in Seyfert galaxies as discovered by high resolution spectroscopic observations recently performed with grating spectrometers on–board of *XMM–Newton* and *Chandra*. They indeed resolved the complex structure of the AGN circumnuclear absorbing material into a multi–phase plasma with several orders of magnitude spread in ξ and systematic blueshifts (Blustin et al. 2003; Kaastra et al. 2002). This observational evidence leads to interpret the warm absorber phenomenon essentially in terms of a photoionized outflowing wind consisting of different inhomogeneous co–existing regions (or shells) characterized by a broad distribution in ξ, temperature and density (Krolik 2002; Behar et al. 2003; Elvis 2000).

Interestingly, while our best–fit values for ionization parameters of the two absorbing components are similar to those found in other Seyfert 1 galaxies (Kaastra et al. 2002; Blustin et al. 2003), the corresponding column densities ($N_H^{T5} \approx 9 \times 10^{22}$ cm^{-2} and $N_H^{T4} \approx 2 \times 10^{22}$ cm^{-2}) are amongst the highest seen by *Chandra* and *XMM–Newton* so far.

Given these high values of N_H, photoionization edges are expected to dominate the absorption features in MKN 304. In fact, at high column densities the UTA absorption lines saturate. Edges (alongside with $2p-nd$ (with $n > 3$) absorption lines) provide the major contribution to the absorption spectrum (Behar, Sako & Kahn 2001). Furthermore as shown in Fig. 1, the absorption feature in MKN 304 is remarkably broad and deep and, hence, hard to reconcile with what simply expected from UTA[3].

Besides absorption, also emission lines are expected to arise from the warm medium. Due to the underlying illuminating bright continuum and the forest of absorption lines such emission features are however difficult to detect in low–resolution data. In particular He–like triplets of O and Ne are usually expected. The OVII line detected at 0.57 keV in the spectrum of MKN 304 is therefore consistent with reprocessing in the warm gas.

However, in sources showing both absorption and emission lines the former usually appear to have different velocities respect to the latter (and in many cases consistent with the galaxy rest–frame, e.g. Collinge et al. 2001), so it is not clear if emitter and absorber systems are intrinsically the same. For instance, Kaastra et al. (2002) found the optical Narrow Line Region as the most likely origin of OVII and Ne IX emission lines observed in NGC 5548. Unfortunately, *EPIC* data do not have enough resolution to shed light on this issue.

We used CLOUDY (Ferland 2001) to further test the idea of a possible origin of the oxygen emission line from the same *warm* medium responsible of the absorption in MKN 304. We employed the table "AGN" ionizing continuum, with an X–ray photon index fixed to 1.88, a hydrogen column density set to 9×10^{22} cm^{-2}, and an ionization parameter equivalent to the highest one obtained from XSPEC. For this high ionization state of the gas, the transmitted X-ray spectrum is only marginally dependent on the gas density, the EUV continuum and the UV/X-ray flux ratio. Following the results of the XSPEC fits, the total output spectrum from CLOUDY has been computed as the sum of the incident and transmitted spectra with relative contributions of 5 and 95%, respectively. In this composite spectrum the most prominent emission feature is due to OVII, whose EW (~ 110 eV) is in excellent agreement with that inferred by our fit, i.e. EW = 105±18 eV. Other emission features in the model (i.e. NeIX, NVI, MgXI) are several times weaker, except for the Fe Kα line, whose EW is similar to that of OVII (see Sect. 4.3.). Therefore, we conclude that although this result does not ultimately proof the origin of the He–like oxygen line in the warm absorber, it clearly supports such a scenario.

Finally, the combination of an unreddened continuum in the optical band (Hα/Hβ ~ 3; e.g. Osterbrock 1977) and a column density of $N_H \sim 10^{23}$ cm^{-2} suggests a dust–free X–ray absorbing medium in MKN 304, maybe located within the dust sublimation radius (see Crenshaw, Kramer & George 2003 and references therein).

4.2 Soft excess

The soft excess component (whose normalization is $\approx 4\%$ of the primary emission) detected in MKN 304 appears similar to that observed in many X–ray obscured objects (Turner et

[3] Nonetheless, it is also worth noting that the colder ionized component has values of N_H, ξ and T approximately consistent with the production of UTA features around 0.75 keV. Unfortunately, the lack of an adequate energy resolution does not allow us to further test this hypothesis.

al. 1997). There are two possibilities to explain the origin of such excess, i.e: scattered/reflected emission from the photoionized gas in the warm absorber and "partial–covering". We discuss in turn these hypothesis in the following.

XMM–Newton and *Chandra* results on Seyfert 2 galaxies (Sako et al. 2002 and reference therein) suggest that the soft X–ray emission in these objects is the result of primary continuum scattering underlying a blend of strong emission lines, mostly from H– and He–ions of C, N, O, Ne, and Fe. Since warm absorber regions show physical properties (i.e. ξ, column densities, temperatures) similar to those observed in the X–ray photoionized emitting plasma in Seyfert 2 galaxies, it is likely that they are different manifestations of the same phenomenon (Kinkhabwala et al. 2002) simply seen at different inclination angles. Within this scenario the soft excess found in MKN 304 would be therefore due to scattered/reflected emission from the ionized outflowing plasma.

Interestingly, Ogle et al. (2000), Bianchi et al. (2003) and Iwasawa et al. (2003) detected indeed an extended soft X–ray emission dominated by narrow emission lines overlapping the optical Narrow Line Region in NGC 4151, NGC 5506 and NGC 4388, respectively. According to this hypothesis, a significant contribution from this extended soft X–ray component to the OVII emission line would be also expected (see Sect. 4.1).

An alternative explanation of this "soft excess" could also be some fraction of the primary continuum leaking through the clumpy obscuring material (i.e. along the line of sight the absorber does not completely cover the nuclear source): the so–called "partial-covering" scenario. Furthermore, as mentioned in Sect. 4.1, clumpiness in the ionized absorbing gas appears to be very likely.

Unfortunately, the present data do not allow to discriminate these hypothesis. The unabsorbed power law in model E (with a slope identical to the primary continuum one) can be therefore considered as a good approximation of the real (more complex) spectrum. However, given the energy resolution of *EPIC* CCD cameras and the relatively faintness of MKN 304, a description of this soft X–ray component in terms of many discrete emission features, as observed in the high resolution spectra of some bright AGNs (see Kinkhabwala et al. 2002), cannot be ruled out.

Finally we rule out the hypothesis of an origin of the soft excess from reprocessing (i.e. reflection) by an ionized disk since this interpretation is inconsistent with the observed centroid of the iron line. In fact, assuming that the line arises from such an ionized disk (as expected if a strong relection component is present; Ross, Fabian & Young 1999), it should be emitted at energy higher than 6.4 keV from iron at high ionization states. On the contrary, we found an energy of the Fe Kα emission line strictly consistent only with "neutral iron" (see below).

4.3 Iron line

We report the first clear evidence of an iron fluorescence emission line around 6.4 keV in the spectrum of MKN 304. The detection of a Fe Kα line at E = 6.34$\pm$0.06 keV constrains the ionization parameter of the emitting medium to be $\xi \lesssim 100$ erg cm^{-2} s^{-1}, higher values of ξ would indeed produce a feature peaked at higher energies (Kallman & McCray 1982) excluded by the present data. Interestingly, both cold and hot warm absorber components that resulted in our best fit (model E) to the *EPIC* spectrum have values of ξ which match well with this constraint. This suggests that a significant component of the iron emission line may be originated in the warm medium.

We have run the same CLOUDY model as in Sect. 4.1 to predict the strength of the Fe Kα emission line. The expected value ($\approx$ 110 eV) falls in the range we measured from the *XMM–Newton* spectrum (i.e. EW = 79$\pm$35 eV). So, interestingly, the iron line detected in MKN 304 is consistent with an origin in the warm absorber observed in this source.

We have also tried to fit the data with a model including a neutral reflection Compton component (**pexrav** model in XSPEC) in order to test a possible origin of the iron line from the optically–thick accretion disk. This spectral parametrization yielded a good fit with a $\chi^2(\nu) = 335(357)$: however, there is no statistical improvement respect to Model E. Although the detection of cold reflection results therefore only marginal, we cannot rule out its presence. The observed spectral range (0.3–12 keV) of this *EPIC* observation is not adequate to constrain the strength of this "bump–like" reprocessed emission feature peaked at $\approx$ 30–40 keV (Lightman & White 1988). The resulting upper limit for the covering factor of the material irradiated by the X–ray source is $R \equiv \Omega/2\pi < 0.7$. Both the value of the equivalent width of the line and R suggest that the reflector – if existing – subtends a solid angle of $\lesssim \pi$ steradian to the X–ray source, i.e. intercepts $\lesssim$ 50% of the primary continuum once a slab geometry for the reflecting medium is assumed (George & Fabian 1991).

Furthermore the narrow profile of the Fe Kα line ($\sigma_{K\alpha}$ <0.18 keV corresponding to Δv(FWHM) $\lesssim$ 8000 km/s for the line velocity width) implies that even if the reprocessing medium is the accretion disk, the fluorescence does not take place from its innermost (relativistic) regions. A substantial contribution to the Fe Kα emission could be provided from the putative molecular torus located at 1–10 pc from the central X–ray source as invoked in the Unification model of AGNs (Antonucci 1993). In this case the material is assumed to be Compton–thick (i.e. with $N_H \gtrsim 1.5 \times 10^{24}$ cm^{-2}, see Matt, Guainazzi & Maiolino 2003), and the emission is due to the reflection of the primary continuum off the inner walls of the torus into our line–of–sight (Ghisellini et al. 1994).

The observed properties of the Fe Kα line in MKN 304 appear to be very similar to the results obtained by the spectral analysis of the brightest Seyfert 1 galaxies using *XMM–Newton* (Pounds & Reeves 2002) and *Chandra* (Padmanabhan & Yaqoob 2002) data. These works indeed shows the "ubiquitous" presence of a narrow iron line component centered at 6.4 keV with an EW $\approx$ 50–100 eV and $\sigma_{K\alpha}$ <120 eV in the X–ray spectra of the low–luminosity (i.e. with $L_{2-10} < 10^{45}$ erg s^{-1}) AGNs.

5 SUMMARY

The $\sim$30 ks *XMM–Newton* exposure presented here is the first X–ray broad–band (0.3–12 keV) observation of MKN 304. Our data analysis has revealed that this Seyfert 1 galaxy has a complex spectrum, dominated by heavy ion-

ized obscuration. This warm absorber can be well fit by a "two–zone" gas with ionization parameter of $\xi \approx 6$ erg cm^{-2} s^{-1} and $\xi \approx 90$ erg cm^{-2} s^{-1}, respectively. We estimate that the warm absorber has a column density of $N_H \approx 9 \times 10^{22}$ cm^{-2} in the high–ionization component and $N_H \approx 2 \times 10^{22}$ cm^{-2} in the low–ionization component. Such values are currently amongst the largest ones observed so far in Seyfert 1 galaxies by *XMM–Newton* and *Chandra*.

A particularly interesting result of our analysis is the detection of an emission feature at ≈ 0.57 keV, likely due to the helium–like oxygen from the warm absorber itself or regions much farther out from the central BH (i.e. the optical Narrow Line Region).

We also report the first detection (significant at 99.9%) of an iron line in this source. The combination of the energy centroid (≈ 6.4 keV) and the upper limit of the line width ($\sigma_{K\alpha} < 0.18$ keV) suggests an origin from "cold" (i.e. FeI–XV) matter distant from the inner disk region. Alternatively, the line strength is consistent with the emission arising from the warm absorber itself.

Finally, we have also found a weak (4% of the primary continuum) soft excess. The presence of this excess could be explained by either emission/scattering from a warm gas or partial covering, or a combination of them.

ACKNOWLEDGMENTS

We thank the anonymous referee for careful reading and helpful comments. We are grateful to all the members of the *XMM–Newton* team for their great efforts in performing the observations and supporting the data analysis. This paper is based on observations obtained with *XMM–Newton*, an ESA science mission with instruments and contributions directly funded by ESA Member States and the USA (NASA). This research has made use of the NASA/IPAC Extragalactic Database (NED) which is operated by the Jet Propulsion Laboratory, California Institute of Technology, under contract with the National Aeronautics and Space Administration.

When our paper was in an advanced stage of the refereeing process we became aware of the publication of a paper by Brinkmann et al. (2004) which discusses the same observation. Their results are broadly consistent with ours insofar as they found strong evidence for ionized material along the line of sight. However, the application of the high background filtering procedure described in the Appendix allowed us to provide a more detailed description of the emission and absorption features in the spectrum. In particular, this leads us to unveil significant evidence for a multizone warm absorber in MKN 304

REFERENCES

Antonucci R.R.J., 1993, ARA&A, 31, 473
Arnaud K.A., 1996, in Jacoby G.H., Barnes J., eds, ASP Conf. Ser. Vol. 101, Astronomical Data Analysis Software and Systems V. Astron. Soc. Pac., San Francisco, p. 17
Avni Y., 1976, ApJ, 210, 642
Behar E., Sako M., Kahn S. M., 2001, ApJ, 563, 497
Behar E., Rasmussen A. P., Blustin A. J., Sako M., Kahn S. M., Kaastra J. S., Branduardi-Raymont G., Steenbrugge K., 2003, ApJ, 598, 232
Bennett C.L., et al., 2003, ApJS, 148, 1
Bianchi S., Balestra I., Matt G., Guainazzi M., Perola G.C., 2003, A&A, 402, 141
Blustin A.J., et al., 2003, A&A, 403, 481
Brinkmann W., Papadakis I.E., Ferrero E., 2004, A&A, 414, 407
Clavel J., Joly M., 1984, A&A, 131, 87
Clements, E.D., 1981, MNRAS, 197, 829
Collinge M.J., et al., 2001, ApJ, 557, 2
Crenshaw D.M., Kraemer S.B., Boggess A., Maran, S.P., Mushotzky R.F., Wu C., 1999, ApJ, 516, 750
Crenshaw D.M., Kraemer S.B., George I.M., 2003, ARA&A, 41, 117
Dickey J.M., Lockman F.J., 1990, ARA&A, 28, 215
Done C., Mulchaey J.S., Mushotzky R.F., Arnaud K.A., 1992, ApJ, 395, 275
Elvis M., 2000, ApJ, 545, 63
Ferland G.J., 2001, a Brief Introduction to Cloudy, Univ. of Kentucky, Department of Physics and Astronomy Internal Report
George I.M., Fabian A.C., 1991, MNRAS, 249, 352
Ghisellini G., Haardt F., Matt G., 1994, MNRAS, 267, 743
Halpern J.P., 1984, ApJ, 281, 90
Iwasawa K., Wilson A.S., Fabian A.C., Young A.J., 2003, MNRAS, 345, 369
Jansen F., et al., 2001, A&A, 365, L1
Kaastra J. S., Steenbrugge K. C., Raassen A. J. J., Van der Meer R. L. J., Brinkman A. C., Liedahl D. A., Behar E., De Rosa A., 2002, A&A, 386, 427
Kallman T.R., McCray R., 1982, ApJS, 50, 263
Kaspi S., et al., 2001, ApJ, 554, 216
Kinkhabwala A., et al., 2002, ApJ 575, 732
Kriss G.A., 2002, in Crenshaw D.M., Kraemer S.B., George I.M., eds, ASP Conf. Ser. Vol. 255, Mass Outflow in active Galactic Nuclei: New Perspectives. Astron. Soc. Pac. San Francisco, 79
Kriss G.A., Canizares C.R., Ricker G.R., 1980, ApJ, 242, 492
Krolik J.H., 2002, MPE Report, 279, 131, (astro-ph/0204418)
Lightman A.P., White T.R., 1988, ApJ, 335, 57
Loiseau N., XMM-Newton Science Analysis System Users Guide, v2.1
Lumb D.H., Warwick R.S., Page M., De Luca A., 2002, A&A, 389, 93
Makishima K., 1986, Lecture Notes in Physics, 266, 246
Malizia A., Bassani L., Stephen J.B., Di Cocco G., Fiore F., Dean A.J., 2003, ApJ, 589, L17
Matt G., Guainazzi M., Maiolino R., 2003, MNRAS, 342, 422
Morrison R., McCammon D., 1983, ApJ, 270, 119
Mushotzky R.F., Done C., Pounds K.A., 1993, ARA&A, 31, 717
Nandra K., Pounds K.A., 1994, MNRAS, 268, 405
Nandra K., George I.M., Mushotzky R.F., Turner T.J., Yaqoob T., 1997, ApJ, 477, 602
Netzer H., et al., 2003, ApJ, 599, 933
Ogle P.M., Marshall H.L., Lee J.C., Canizares C.R., 2000, ApJ, 545, L810

Osterbrock D.E., 1977, ApJ, 215, 733
Padmanabhan U., Yaqoob T., 2002, in Li X.D., Trimble V., Wang Z.R., eds, IAU Symp. 214, High Energy Processes and Phenomena in Astrophysics. Astron. Soc. Pac., San Francisco, (astro-ph/0211386)
Pan H.C., Stewart G.C., Pounds K.A., 1990, MNRAS, 242, 177
Piconcelli E., Cappi M., Bassani L., Di Cocco G., Dadina M., 2003, A&A, 412, 689
Pounds K.A., Reeves J.N., 2002, in Jansen F., ed., Proc. New Visions of the X-ray Universe in the XMM-Newton and Chandra Era. ESTEC, Netherlands (astro-ph/0201436)
Rachen J.P., Mannheim K., Biermann, P.L., 1996, A&A, 310, 371
Reynolds C.S., 1997, MNRAS, 286, 513
Reynolds C.S., Fabian A.C., 1995, MNRAS, 273, 1167
Ross R.R., Fabian A.C., Young A.J., 1999, MNRAS, 306, 46
Sako M., et al., 2002, MPE Report, 279, 191
Struder L., et al., 2001, A&A, 365, L18
Tananbaum H., Peters G., Forman W., Giacconi R., Jones C., Avni Y., 1978, ApJ, 223, 74
Turner M.J.L.T., Abbey A., Arnaud M., et al., 2001, A&A, 365, L27
Turner T.J., Nandra K., George I.M., Fabian A.C., Pounds K.A., 1993, ApJ, 419, 127
Turner T.J., George I.M., Nandra K., Mushotzky R.F., 1997, ApJS, 113, 23

APPENDIX A: HIGH BACKGROUND FILTERING PROCEDURE

XMM–Newton experiences high "flaring" background periods due to the crossing of clouds of high–energy particles (mainly soft protons), which are focussed through the mirrors to the detectors (Lumb et al. 2002). Time intervals affected by background flares are essentially useless for the scientific analysis. The standard method to filter out these high background periods consists in rejecting periods of high count rate (CR) at energies $\gtrsim$ 10 keV (see *XMM–Newton* Science Analysis System Users Guide v2.1; Loiseau 2003). The recommended thresholds for the background count rate are 0.35 count/s and 1 count/s for the MOS and the PN camera, respectively. This approach (i.e. using fixed threshold for the CR of the background) well adapts for the detection of faint sources but it could produce very conservative results in the case of high–flux sources.

In the reduction of the MKN 304 data, we thus apply the following alternative procedure ("MaxSNR" hereafter) to reject the high background level periods. The underlying idea basically consists of filtering out just those time intervals for which the count rate of the background reach values so high that the SNR of the source does not significantly improve (or even worses) by including such time intervals in the analysis. To this aim, lightcurves of the source and background region, i.e. a proper annulus around the source large enough to provide a good estimation of the background (with a 120 arcsec radius in the case of MKN 304), are extracted in the energy band for which the SNR should to be maximized. In the analysis of MKN 304 data, we have taken into account the 0.5–1.3 keV (0.6–1.3 keV) band for *PN*(*MOS*) in order to optimize the SNR in the band where most of the prominent warm absorber features are located.

On the contrary, the "standard" filtering method requires to extract a lightcurve of the entire field of view for energies above $E > 10$ keV.

Lightcurve datapoints for the source and background are sorted for increasing values of the CR of the background region. The cumulative signal–to–noise (SNR_{cum}) distribution function is then calculated.

The SNR_{cum} as a function of the increasing background CR builds a curve which monothonically rises up to a peak. After this maximum value, the SNR_{cum} distribution indeed flattens or even decreases. This value is the threshold used to reject the high background periods. In fact, if included, these periods would not provide any significant improvements to the final SNR of the spectrum of the source, but it would increase the background contribution to the raw source spectrum.

This method to filter out high background periods optimizes the duration of the observation useful for a meaningful scientific analysis on the basis of the ratio between the count rates of source and background. It appears particularly appealing in the case of bright source for which an even "flaring" background can represent just a negligible fraction of their CR. It also has the advantage that the

	Standard method	MaxSNR method
Final exposure	6.7 ks	29 ks
Obs. countrate	0.50 ±0.01	0.480 ±0.005
SNR	53	103
Total counts (0.3–12 keV)	2971	16077

Table A1. Comparison between the results obtained applying the "standard" method and the "MaxSNR" method presented in this paper for the high background filtering in MKN 304. Data are reported for the *PN* camera.

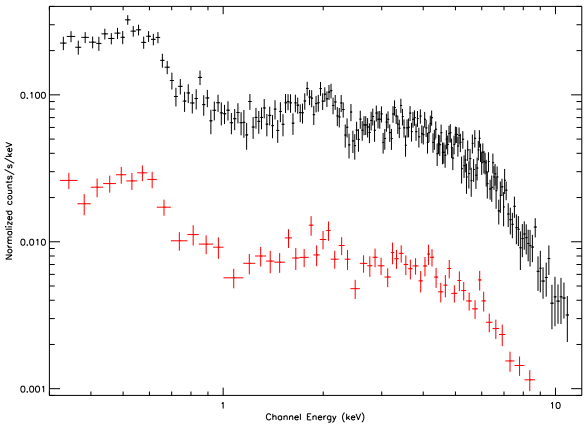

Figure A1. Comparison between the *PN* spectrum of MKN 304 obtained using the MaxSNR filtering method (*top*) and the standard filtering procedure (*bottom*). After the filtering the exposure times result of 29 ks and 6.7 ks, respectively.

filtering is performed in a particular energy band (chosen *a priori*) where the SNR need be maximized for the accurate study of peculiar spectral features.

Table A1 lists the final values of exposure, total counts in the 0.3–12 keV band, countrate and SNR for the *PN* camera obtained using the "MaxSNR" method compared to those derived from the application of the "standard" method. In particular, the method presented here yields a number of counts which is about 5.5 times larger than that resulted from the "standard" method. Fig. A1 shows the comparison between the spectra obtained using the two filtering procedures: the higher quality of the *PN* spectrum provided by the "MaxSNR" method is clearly evident.

This paper has been typeset from a TEX/ LATEX file prepared by the author.